Al_2O_3/TiO_2 nano-pattern antireflection coating with ultralow surface recombination

P. Spinelli,[1,a)] B. Macco,[2] M. A. Verschuuren,[3] W. M. M. Kessels,[2] and A. Polman[1]
[1]*Center for Nanophotonics, FOM Institute AMOLF, Amsterdam, The Netherlands*
[2]*Eindhoven University of Technology, Eindhoven, The Netherlands*
[3]*Philips Research Laboratories, Eindhoven, The Netherlands*

(Received 22 April 2013; accepted 29 May 2013; published online 11 June 2013)

We present a nano-patterned dielectric coating for crystalline Si solar cells that combines excellent anti-reflection and passivation properties. The nano-patterned coating comprises an array of TiO_2 nanocylinders placed on top of an ultra-thin Al_2O_3 layer on a flat Si(100) wafer. The antireflection effect stems from the preferential forward scattering of light through leaky Mie resonances in the TiO_2 nanocylinders. The Al_2O_3 layer provides excellent passivation of the Si surface. We experimentally demonstrate ultralow surface recombination with carrier lifetimes above 4 ms, combined with a reflectivity of 2.8% averaged over a broad spectral range.
© *2013 AIP Publishing LLC*. [http://dx.doi.org/10.1063/1.4810970]

Antireflection (AR) coatings and passivation layers are essential components in solar cells. The former are used to reduce unwanted reflection of light from the surface of the solar cell, whereas the latter are used to reduce surface carrier recombination.[1] Standard AR approaches for crystalline Si (c-Si) based devices include transparent dielectric layers,[2] micron-sized pyramidal surface texturing,[3] and graded-index tapered nanostructures.[4–6] These techniques however present drawbacks such as limited spectral and angular range of operation, increase of surface area and thus increase of surface recombination, and unsuitability for application to ultra-thin (less than 20 μm) wafers. Recently, we have shown that nano-sized dielectric (Mie) nano-scatterers can be used to achieve broadband omnidirectional low reflectivity for c-Si wafers.[7] An array of Si nano-cylinders (NCs) etched into the surface of a Si wafer reduces the reflectivity of the wafer down to 1.3% in the visible spectral range, and for angles of incidence up to 60°. The mechanism behind the reduced reflectivity is the preferential forward scattering of the incident light through leaky Mie resonances in the dielectric nanoparticles.[8,9] While this geometry leads to ultra-low reflectivity, a key question is how it affects surface recombination due to both the increased surface area and possible etch-induced damage during the Si NC fabrication. To study this, we fabricate arrays of Si NCs on top of a double-side polished 270-μm-thick float-zone (FZ) Si wafer and deposit a 30-nm-thick Al_2O_3 passivation layer. Al_2O_3 is well known for its passivation properties[10] and has been used to passivate reactive-ion etched Si surfaces.[11] The Si NC array is fabricated using substrate-conformal imprint lithography (SCIL) and reactive ion etching (RIE), similarly to Ref. 7. The Al_2O_3 passivation layer was deposited by plasma-assisted atomic layer deposition (ALD) at 200 °C, followed by annealing at 400 °C for 10 min in N_2 environment. Figure 1(a) shows a scanning electron microscope (SEM) image of the array of Si NCs after the Al_2O_3 deposition, imaged with a tilt angle of 45°. The inset shows a focused ion beam (FIB) cross-section of two Si NCs, conformally coated with 30 nm Al_2O_3.

Figure 1(b) shows the minority carrier lifetime as a function of the injected carrier density, measured in a Sinton WCT-100 lifetime tester. The graph shows data for an unpassivated (dashed red line) and passivated (solid red) flat Si wafer (reference samples), and for an unpassivated (dashed blue) and passivated (solid blue) Si wafer with Si NC array, illuminated from the side of the Si NCs. The reference measurements clearly show the beneficial effect of the Al_2O_3 layer on the surface passivation of a flat Si wafer. For injected carrier densities of 10^{15} cm^{-3}, the carrier lifetime is improved from 3 μs (black) to 1 ms (red) by applying the Al_2O_3 passivation layer. On the other hand, the sample with Si NCs shows only a small improvement in carrier lifetime upon passivation, from 3 μs (purple) to 8 μs (blue).

Figure 1 shows that the deposition of a standard ALD alumina passivation layer on the surface of the Si Mie NC is not effective in reducing surface recombination. In this paper, we present an alternative dielectric nano-patterned Mie AR coating which is fully compatible with a standard Al_2O_3 passivation layer. This Mie coating comprises a TiO_2 NC array fabricated on top of a flat, Al_2O_3-passivated Si wafer. We demonstrate that this combined geometry yields ultralow surface recombination velocities and excellent AR properties. Carrier lifetimes up to 4 ms were measured, together with an average reflectivity weighed over the AM1.5 solar spectrum in the 420–980 nm spectral range of 2.8%.

Figure 2(a) shows a schematic of the AR coating and passivation geometry. A square array of TiO_2 nano-cylinders (500 nm pitch) is made on top of a flat 50-nm-thick TiO_2 spacer layer. The TiO_2 cylinders have a diameter of 350 nm and height of 100 nm. From numerical simulations, it was found that this geometry yields the optimal anti-reflection properties. The TiO_2 Mie-coating is made on a Si substrate coated with a 5-nm-thick Al_2O_3 passivation layer. Numerical simulations show that, in order to achieve reflectivities below 3%, an Al_2O_3 layer with thickness below 10 nm must be used underneath the TiO_2 Mie coating. For such thin Al_2O_3 layers, plasma-assisted ALD is preferable to thermal ALD in order to achieve excellent surface passivation.[10]

a)Author to whom correspondence should be addressed. Electronic mail: spinelli@amolf.nl

Downloaded 15 Aug 2013 to 194.171.111.64. This article is copyrighted as indicated in the abstract. Reuse of AIP content is subject to the terms at: http://apl.aip.org/about/rights_and_permissions

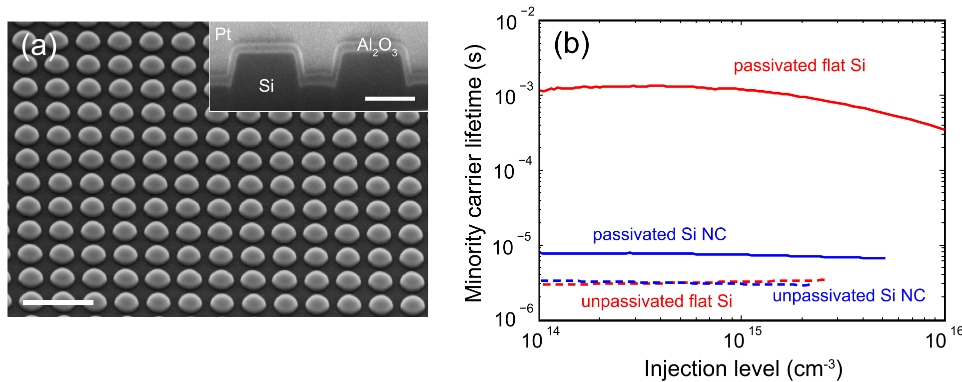

FIG. 1. (a) SEM image of the Si NC array, coated with 30 nm Al_2O_3 (scale bar: 1 μm). The inset shows a FIB cross section of two Si NCs (scale bar: 200 nm). (b) Carrier lifetime as a function of injected carrier density, for an unpassivated (dashed red) and passivated (solid red) flat Si reference, and for an unpassivated (dashed blue) and passivated (solid blue) Si wafer coated with Si NCs.

Double-side polished n-type FZ ⟨100⟩ wafers, with a thickness of 270 μm and resistivity of 2.5 Ω cm, were used for the experiments. The native oxide is removed by a 1 min dip in a 1% dilute HF solution. The Al_2O_3 passivation layer is then deposited on both sides of the wafer using plasma-assisted ALD at 200 °C, followed by a rapid thermal anneal (RTA) treatment at 400 °C for 10 min in a N_2 environment. Spectroscopic ellipsometry was performed to determine the Al_2O_3 and interfacial SiO_2 layer thicknesses, which were found to be 5 nm and 2 nm, respectively. A 50-nm-thick TiO_2 layer is then deposited using electron beam evaporation from a TiO_2 source. Afterwards, the sample is coated with a PMMA/sol-gel resist, and SCIL is used to imprint a nano-pattern of holes in the sol-gel. A breakthrough RIE using an O_2/N_2 plasma is performed to transfer the hole pattern into the PMMA. The TiO_2 NCs are then fabricated by electron beam evaporation from a TiO_2 source followed by lift-off of the resist. Figure 2(b) shows a FIB cross section of the final sample. The left panel shows an overview of the FIB cross section, showing the Si substrate, the array of the TiO_2 NCs, and a platinum top layer deposited to protect the array during the FIB milling. The top-right panel shows the cross section of a single TiO_2 nanoparticle on top of the TiO_2 and Al_2O_3 layers. The bottom-right panel is a cross section showing the flat TiO_2 and Al_2O_3 layers, imaged in between two NCs. The thicknesses of these two layers derived from the image are 48 nm and 6 nm, respectively. Figure 2(c) is a SEM overview of the TiO_2 NC array, showing the uniformity of the SCIL-imprinted surface. Figure 2(d) shows the surface morphology as probed by AFM, which was used to characterize the TiO_2 nanoparticle size and shape. The figure shows that the nanoparticles have a tapered cylindrical shape, with a lower diameter of 380 nm, an upper diameter of 350 nm and height of 85 nm. The nanoparticles are surrounded by a 20-nm-thick "halo" ring at the bottom. This will be discussed further on.

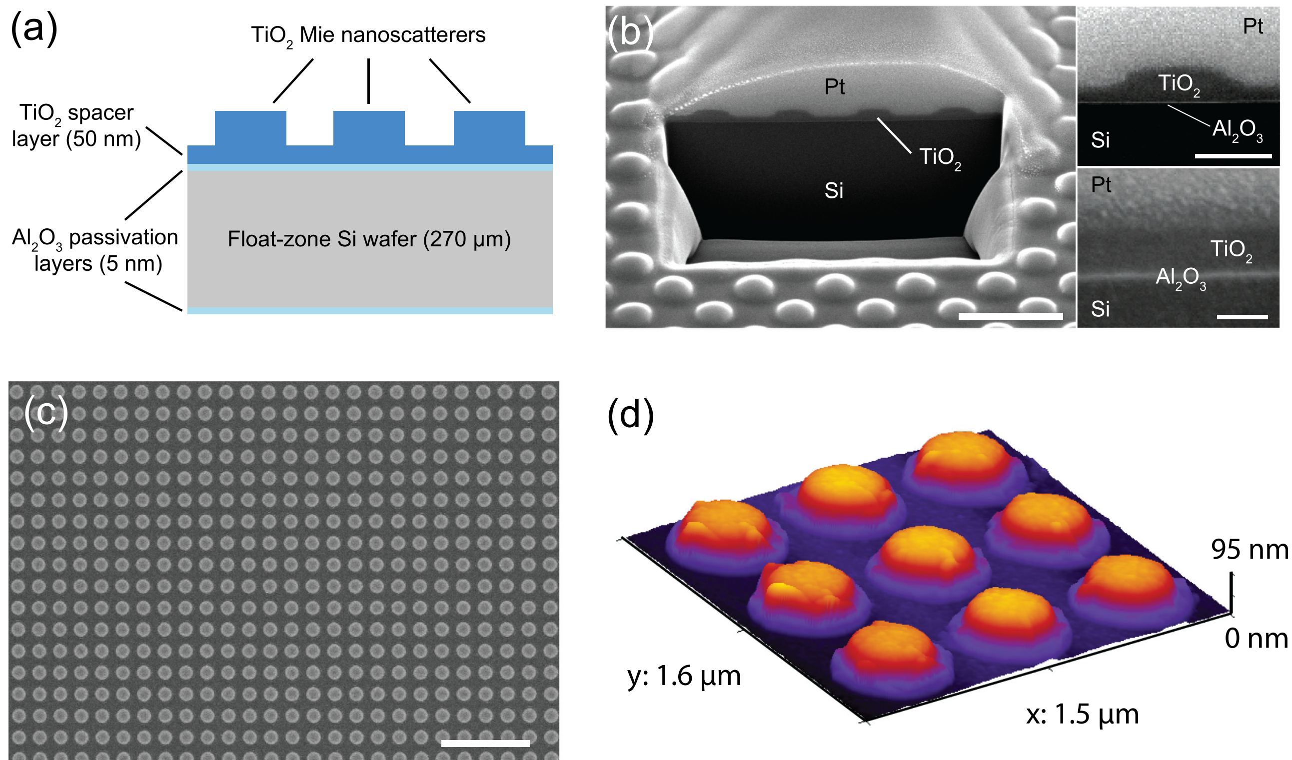

FIG. 2. (a) Schematic of the TiO_2-based Mie coating. (b) FIB cross section of the experimental sample. Scale bars: 1 μm in the left panel, 300 nm in the top-right panel, and 50 nm in the bottom-right panel. (c) SEM top-view of the TiO_2 NC array. Scale bar is 2 μm. (d) Surface morphology of the TiO_2 NC array as probed by AFM.

Downloaded 15 Aug 2013 to 194.171.111.64. This article is copyrighted as indicated in the abstract. Reuse of AIP content is subject to the terms at: http://apl.aip.org/about/rights_and_permissions

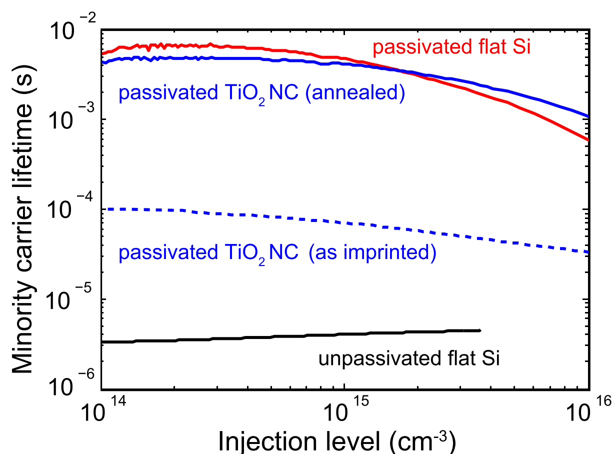

FIG. 3. Carrier lifetime as a function of injected carrier density, for an unpassivated (black) and passivated (red) flat Si wafers, and for a passivated Si wafer with a TiO_2 Mie coating, before (dashed blue) and after (solid blue) rapid thermal annealing at 400 °C in N_2.

Figure 3 shows the minority carrier lifetime as a function of injected carrier concentration for a flat unpassivated Si wafer (black), a flat Si wafer passivated with 5 nm Al_2O_3 (red), a Si wafer passivated with 5 nm Al_2O_3 and coated with TiO_2 NCs (dashed blue line), and the same wafer after applying a post-fabrication RTA treatment at 400 °C for 15 min in N_2 environment (solid blue). Similarly to Fig. 1(a), this graph shows that the poor lifetimes of an unpassivated reference Si wafer are drastically improved by the deposition of the Al_2O_3 passivation layer. For injected carrier densities of 10^{15} cm^{-3}, carrier lifetimes up to 5 ms (red line) are achieved by using an Al_2O_3 layer thickness of only 5 nm. After the fabrication of the TiO_2 NCs, a drastic reduction in carrier lifetime is observed (80 μs, dashed blue line). We attribute this mainly to defects in the Al_2O_3 passivation layer that are induced by the vacuum-UV radiation by the RIE plasma used to fabricate the TiO_2 NCs.[12] Sub-surface ion damage in Si due to the RIE may also contribute to degrading the carrier lifetimes. However, very good lifetimes above 1 ms are observed after a post-fabrication RTA treatment at 400 °C is performed. An optimal post-anneal time of 15 min is found at this temperature, yielding lifetimes as high as 4.1 ms for injected carrier densities of 10^{15} cm^{-3}. This lifetime is so high that can only be measured on high-quality FZ-Si wafers. It corresponds to a maximum effective surface recombination velocity of only 3.3 cm/s.

The samples were characterized by total optical reflectivity measurements performed in an integrating sphere setup, with an angle of incidence of 5° off the surface normal. Figure 4(a) shows the measured total reflectivity spectrum for a flat uncoated Si wafer (black) and for an Al_2O_3-passivated Si wafer with the TiO_2 Mie coating (solid red line). The experimental data show a broadband reduction of reflectivity over the entire 420–980 nm spectral range for the TiO_2 Mie coating with respect to the bare Si wafer. This is due to the strong forward scattering from Mie resonances of the TiO_2 nanoparticle.[7] From numerical simulations, we found that the TiO_2 nanoparticle scattering cross section spectrum shows a broad first-order Mie resonance in the spectral range of 500–800 nm. It was also found that this resonance originates from a magnetic dipole-like mode, in

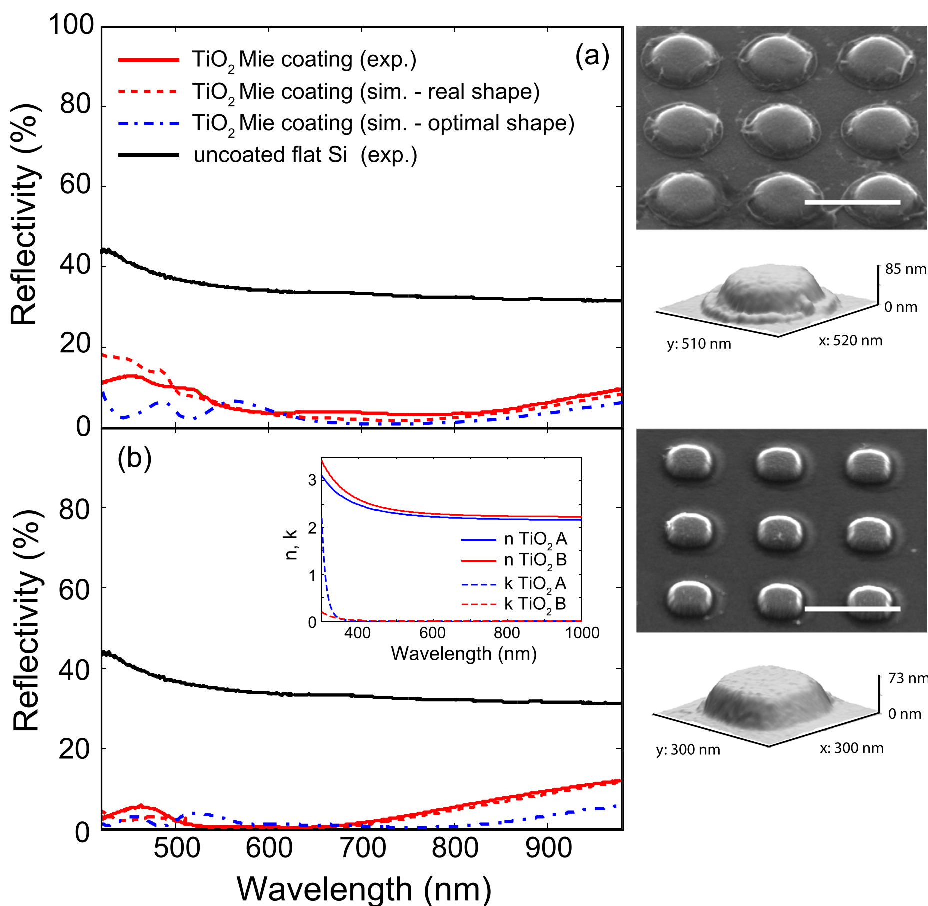

FIG. 4. (a) Measured reflectivity spectra of a bare Si wafer (black) and an Al_2O_3-passivated Si wafer with a TiO_2 Mie coating (solid red). The TiO_2 is deposited by electron beam evaporation from a TiO_2 source. The dashed lines are the simulated reflectivity spectra of an array of TiO_2 nanoparticles, with particle shape given by the AFM data of the experimental sample (dashed red) and with an optimal particle shape (dashed blue). The optimal nanoparticle shape is a cylinder with diameter of 350 nm and height of 100 nm. The insets on the right show a SEM image of the TiO_2 nanoparticle array (top, scale bar is 500 nm) and the AFM image of a single nanoparticle (bottom). (b) Reflectivity spectra measured on a sample fabricated with a different nanoimprint stamp and TiO_2 evaporated using a Ti_3O_5 source. In this case, the optimal nanoparticle dimensions are 300 nm (diameter) and 100 nm (height). The inset shows the optical constants of the TiO_2 evaporated from a TiO_2 source (A), and the TiO_2 evaporated from a Ti_3O_5 source (B). n and k are the real and imaginary part of the refractive index, respectively. The insets on the right show a SEM (top, scale bar is 500 nm) and AFM image (bottom) of the nanoparticles.

Downloaded 15 Aug 2013 to 194.171.111.64. This article is copyrighted as indicated in the abstract. Reuse of AIP content is subject to the terms at: http://apl.aip.org/about/rights_and_permissions

agreement with Ref. 13. The broadband behavior stems from the fact that the Mie resonance of a nanoparticle in proximity of a high index substrate is "leaky," i.e., only few optical cycles occur before light is fully scattered into the substrate. Overall, the AM1.5-averaged reflectivity of a bare Si wafer (32.2%) is reduced to 5.8% by employing the TiO_2 Mie coating. The dashed red line in Fig. 4(a) represents the reflectivity spectrum obtained from Finite Difference Time Domain (FDTD) simulations, using the AFM topography as an input for the particle shape. As can be seen, good agreement is observed between simulated and experimental data. The right panels in Fig. 4(a) show a SEM image of the nanoparticles (top) and the AFM data of a single nanoparticle (bottom). The actual nanoparticle shape is not ideal, due to the presence of a 20-nm-thick "halo" ring at the bottom. Using FDTD simulations, the case of an ideal cylindrical nanoparticle shape with optimal dimensions was also investigated. The results are shown by the dashed blue line in Fig. 4(a). In this case, the AM1.5-averaged reflectivity is found to be 2.8%. For comparison, a double-layer AR coating comprised of a porous (low n) TiO_2 film on top of a dense (high n) TiO_2 film yields an average reflectivity of 6.5%.[14]

Figure 4(a) shows that a cylindrical particle shape with optimal dimensions is crucial in order to achieve the best AR properties. A second sample series was made using a different nanoimprint stamp and different conditions for the breakthrough etch of the PMMA/sol-gel resist (O_2 instead of O_2/N_2 plasma). Furthermore, in this case the TiO_2 was deposited with electron-beam evaporation using a Ti_3O_5 source, in combination with oxygen flow. The right panels in Fig. 4(b) show a SEM image (top) of the nanoparticles fabricated in this way, as well as AFM data of a single nanoparticle (bottom). In this case, a particle shape close to the ideal cylindrical shape was obtained. The nanoparticles have diameter of 250 nm and height of 73 nm, slightly smaller than the optimal dimensions of 300 nm diameter and 100 nm height found with FDTD simulations. Figure 4(b) shows the measured total reflectivity spectrum for a flat uncoated Si wafer (black) and for an Al_2O_3-passivated Si wafer with the TiO_2 Mie coating (solid red line). As in Fig. 4(a)), a broadband reduction is observed for the entire spectral range of 420–980 nm. The average reflectivity of the TiO_2 Mie coating is found to be 2.6%. As before, excellent agreement with the simulated data (dashed red line) is observed. The simulated reflection spectrum for a TiO_2 Mie coating with optimal geometry (dashed blue) yields an average reflectivity as low as 1.6%.

Finally, we discuss the effect of the slightly different optical constants of TiO_2, due to electron-beam evaporation from different source materials. The inset in Fig. 4(b) shows the real (n) and imaginary part (k) of the refractive index of the TiO_2 used in the experiment of Fig. 4(a) (blue, A) and Fig. 4(b) (red, B), measured with spectroscopic ellipsometry. The TiO_2 evaporated using a Ti_3O_5 source (B) has a slightly higher n than the TiO_2 evaporated from a TiO_2 source (A), and a lower k (thus lower absorption) in the spectral range below 400 nm. The higher index leads to a lower simulated reflectivity spectrum (dashed blue line in Fig. 4(b)).

In summary, we have presented a TiO_2-nanoparticle-based coating for crystalline Si solar cells, which combines good surface passivation and anti-reflection properties. Carrier lifetimes higher than 4 ms were measured, by using a 5-nm-thick Al_2O_3 passivation layer placed underneath the TiO_2 nanoparticle coating. Total reflection measurements show a broadband AR effect in the spectral range of 420–980 nm, with an AM1.5-averaged reflectivity of 2.8%. The low reflectivity stems from the preferential forward scattering of Mie resonances in the TiO_2 nanocylinders.

We thank SARA Computing and Networking Services (www.sara.nl) for their support in using the Lisa Compute Cluster. This work is part of the research program of the Foundation for Fundamental Research on Matter (FOM), which was financially supported by the Netherlands Organization for Fundamental Research (NWO). It is also funded by the European Research Council. This work is also part of the Global Climate and Energy Project (GCEP).

[1]M. A. Green, *Solar Cells: Operating Principles, Technology and System Applications* (University of New South Wales, 1998).
[2]J. Zhao and M. A. Green, IEEE Trans. Electron Devices **38**(8), 1925–1934 (1991).
[3]W. H. Southwell, J. Opt. Soc. Am. **8**, 549–553 (1991).
[4]H. M. Branz, V. E. Yost, S. Ward, K. M. Jones, B. To, and P. Stradins, Appl. Phys. Lett. **94**, 231121 (2009).
[5]H.-C. Yuan, V. E. Yost, M. R. Page, P. Stradins, D. L. Meier, and H. M. Branz, Appl. Phys. Lett. **95**, 123501 (2009).
[6]S. Koynov, M. S. Brandt, and M. Stutzmann, Appl. Phys. Lett. **88**, 203107 (2006).
[7]P. Spinelli, M. A. Verschuuren, and A. Polman, Nat. Commun. **3**, 692 (2012).
[8]G. Mie, Ann. Phys. **330**, 377–445 (1908).
[9]T. Coenen, J. van de Groep, and A. Polman, ACS Nano **7**, 1689–1698 (2013).
[10]G. Dingemans and W. M. M. Kessels, J. Vac. Sci. Technol. A **30**(4), 040802 (2012).
[11]M. Otto, M. Kroll, T. Käsebier, R. Salzer, A. Tünnermann, and R. B. Wehrspohn, Appl. Phys. Lett. **100**, 191603 (2012).
[12]H. B. Profijt, P. Kudlacek, M. C. M. van de Sanden, and W. M. M. Kessels, J. Electrochem. Soc. **158**, G88 (2011).
[13]A. I. Kuznetsov, A. E. Miroshnichenko, Y. H. Fu, J. B. Zhang, and B. Luk'yanchuk, Sci. Rep. **2**, 492 (2012).
[14]S. B. Richards, Sol. Energy Mater. Sol. Cells **79**, 369–390 (2003).

Downloaded 15 Aug 2013 to 194.171.111.64. This article is copyrighted as indicated in the abstract. Reuse of AIP content is subject to the terms at: http://apl.aip.org/about/rights_and_permissions